

Biocatalysis, DNA–protein interactions, cytotoxicity and molecular docking of Cu(II), Ni(II), Zn(II) and V(IV) Schiff base complexes

Chithiraivel Balakrishnan¹ | M. Theetharappan¹ | P. Kowsalya¹ | Sathesh Natarajan² |
M.A. Neelakantan¹  | S.S. Mariappan¹

¹Chemistry Research Centre, National Engineering College, K. R. Nagar, Kovilpatti 628503, Thoothukudi District, Tamil Nadu, India

²Department of Pharmacy, School of Health Sciences, Kwazulu Natal University, Durban 4001, South Africa

Correspondence

M. A. Neelakantan, Chemistry Research Centre, National Engineering College, K. R. Nagar, Kovilpatti – 628503, Thoothukudi District, Tamil Nadu, India.
Email: drmaneelakantan@gmail.com

Funding Information

Science and Engineering Research Board (SERB); Department of Science and Technology (DST); Government of India, New Delhi, Grant/Award Number: EMR-II/2014/000081; Board of Research in Nuclear Sciences (BRNS); DAE-BAR, Mumbai, India, Grant/Award Number: 35/14/03/2014

Four mononuclear metal complexes (Cu(II) (**1**), Ni(II) (**2**), Zn(II) (**3**) and V(IV) (**4**)) were synthesized using the Schiff base ligand 2,2'-{cyclohexane-1,2-diylbis[nitrilo(1*E*)eth-1-yl-1-ylidene]}bis[5-(prop-2-yn-1-yloxy)phenol] and structurally characterized by various spectral techniques. The catecholase-mimicking activities of **1–4** were investigated and the results reveal that all the complexes have ability to oxidize 3,5-di-*tert*-butylcatechol (3,5-DTBC) to 3,5-di-*tert*-butylquinone in aerobic conditions. Electrospray ionization mass spectrometry studies were performed for **1–4** in the presence of 3,5-DTBC to determine the possible complex–substrate intermediates. X-band electron paramagnetic resonance spectroscopy results indicate that the metal centres are involved in the catecholase activity. Ligand-centred radical generation was further confirmed by density functional theory calculation. The phosphatase-like activity of **1–4** was investigated using 4-nitrophenylphosphate as a model substrate. All the complexes exhibit excellent phosphatase activity in acetonitrile medium. The interactions of **1–4** with calf thymus DNA (CT-DNA) and bovine serum albumin (BSA) protein were investigated using absorption and fluorescence titration methods. All the complexes strongly interact with CT-DNA and BSA protein. The complexes exhibit significant hydrolytic cleavage of supercoiled pUC19 DNA. Complexes **1–4** exhibit significant *in vitro* cytotoxicity against MCF7 (human breast cancer) and MIA-PA-CA-2 (human pancreatic cancer) cell lines. Moreover, the molecular docking technique was employed to determine the binding affinity with DNA and protein molecules.

KEYWORDS

catecholase activity, cytotoxicity, DNA–protein interactions, metal complexes, phosphatase activity

1 | INTRODUCTION

The catecholase- and phosphatase-like activities of metal complexes are of recent interest due to their importance in the development of new bioinspired catalysts.^[1] The metabolism of catechol is significant from both the biological and environmental perspectives and the conversion of catechol to other species *in vivo* is catalysed by catechol dioxygenase and catechol oxidase.^[2] Catechol oxidase is a copper-

containing protein that catalyses the oxidation of *o*-diphenols to *o*-quinones.^[3] The formed *o*-quinones are auto-polymerized to produce melanin, which protects tissues against pathogens or insects. Hydrolase is a class of metalloenzymes that catalyses the hydrolysis of different types of substrates including phosphate esters (4-nitrophenylphosphate), peptides and nucleic acids.^[4] Therefore we believe that investigating the catecholase- and phosphatase-like activities of metal complexes will produce better biocatalysts.

Metal complexes with suitable geometry, charge on the metal centre, electron density and various ligation sites are capable of binding and inducing the degradation of DNA and proteins. DNA and proteins also have a number of coordination sites including hard oxygen atoms and soft nitrogen atoms. For most anticancer drugs, the primary target molecule is DNA. Metal complexes can bind to DNA via non-covalent interactions such as electrostatic binding, groove binding, intercalative binding and partial intercalative binding.^[5] Metal complex–DNA interaction studies are of great importance for understanding the mechanism of interaction of drugs with biomolecules. Cisplatin is one of the most commonly used metal-based anticancer drugs for cancer therapy, but it has number of side effects.^[6] Hence, major efforts are being made to substitute this drug with suitable alternatives. Furthermore, most of the recent research on clinical agents has revealed that drugs (metal complexes) not only bind to the DNA, but also strongly interact with serum albumin proteins such as bovine serum albumin (BSA) and human serum albumin.^[7] Salen-type ligands and salen-based metal complexes have been reported to bind to DNA and to be capable of cleaving DNA.^[8] Terminal alkyne functionality is widely used in pharmaceuticals and it plays an important role in neuroprotection and shows unique inhibitory properties towards flavin-linked oxidases.^[9]

In continuation of our interest in metal Schiff base complexes,^[10] the present paper reports the synthesis and characterization of Cu(II), Ni(II), Zn(II) and V(IV) complexes with Schiff bases derived from alkyne arms containing acetophenone moiety and *trans*-1,2-cyclohexanediamine. The catecholase- and phosphatase-like activities of the metal complexes were investigated using spectral methods. Investigation of the binding properties of the metal complexes with calf thymus DNA (CT-DNA) and BSA protein was carried out. We determined the cytotoxicity of all the complexes against MCF7 (human breast cancer) and MIA-PA-CA-2 (human pancreatic cancer) cell lines. Molecular docking studies were also carried out for all the complexes to determine their binding affinity with protein and DNA.

2 | EXPERIMENTAL

2.1 | Materials general methods

Trans-1,2-diaminocyclohexane, 2,4-dihydroxyacetophenone, potassium carbonate, metal salts copper acetate, nickel acetate, zinc acetate and vanadium sulfate, 3,5-di-*tert*-butylcatechol (3,5-DTBC), 4-nitrophenylphosphate disodium salt hexahydrate (4-NPP) and tetrabutylammonium perchlorate (TBAP) were purchased from Aldrich and used without further purification. Elemental analyses (CHN) were carried out with a Thermo Finnigan Flash EA 1112 elemental analyser. Fourier transform infrared (FT-IR) spectra were

recorded with a Shimadzu 8400S spectrophotometer using KBr pellets in the range 400–4000 cm⁻¹. Electronic absorption spectra were recorded at room temperature using a UV-2450 spectrophotometer. Emission spectra were recorded with a Jasco FP-8300 spectrofluorophotometer. NMR spectra were recorded in CDCl₃ with a Bruker Avance 400 MHz spectrometer. X-band electron paramagnetic resonance (EPR) spectra were recorded using a Bruker EMX Plus instrument. Electrospray ionization (ESI) mass spectra were recorded with a Bruker-Daltonics microTOF-Q II mass spectrometer. Cyclic voltammograms were obtained with a CHI620E spectroelectrochemical workstation in acetonitrile solutions containing 0.1 M TBAP as supporting electrolyte. The experiments were carried out in a conventional three-electrode cell composed of an Ag/AgCl reference electrode, a platinum wire as auxiliary electrode and glassy carbon as working electrode.

2.2 | Synthetic procedures

2.2.1 | Synthesis of ligand

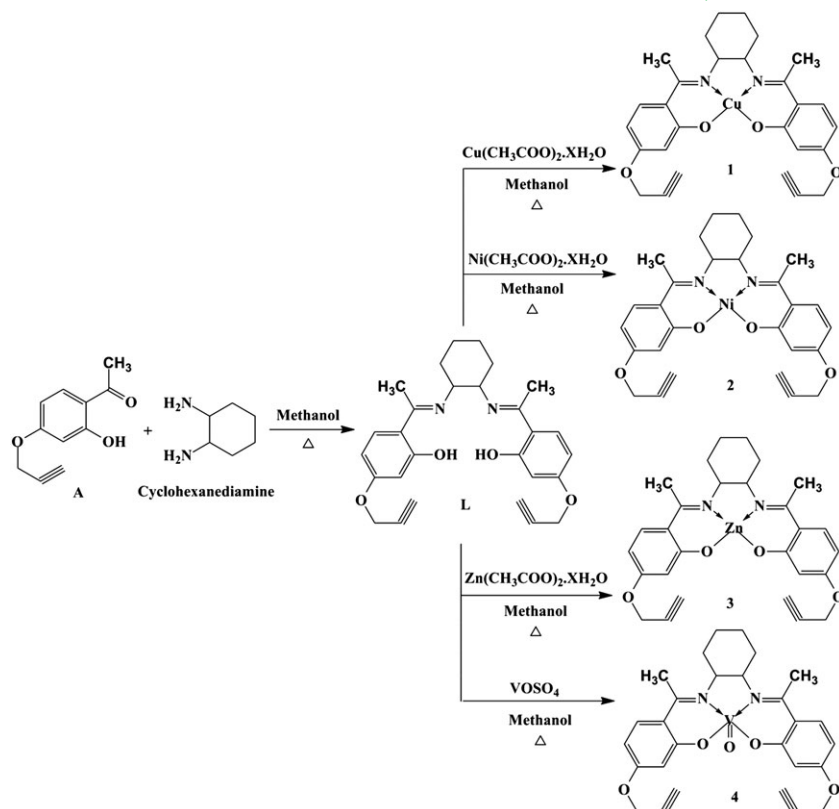
The synthetic procedure for 2,2'-(cyclohexane-1,2-diylbis[nitrilo(1*E*)eth-1-yl-1-ylidene])bis[5-(prop-2-yn-1-yloxy)phenol] (L) was reported in our earlier work.^[11]

2.2.2 | Synthesis of complex 1 (Scheme 1)

A methanolic solution (10 ml) of Cu(OAc)₂·H₂O (0.20 g, 1.0 mmol) was added to Schiff base L (0.46 g, 1.0 mmol) with constant stirring, resulting in the precipitation of a green-coloured compound. The mixture was further refluxed for 1 h. It was then filtered and washed with diethyl ether and dried in a desiccator containing anhydrous CaCl₂. Yield 79%; lavender-coloured solid; m.p. 272 °C. Anal. for C₂₈H₂₈CuN₂O₄ (%): found (calcd): C, 64.65 (64.66); H, 5.42 (5.43); N, 5.36 (5.39). UV–visible (CH₃CN, λ_{max}, nm): 282, 370, 563. FT-IR (KBr, ν, cm⁻¹): 3197 (–C≡C–H), 2931 (asymmetric –C–H), 2849 (symmetric –C–H), 2110 (–C≡C–), 1596 (–C=N). ESI-MS (*m/z*): 537.22.

2.2.3 | Synthesis of complex 2 (Scheme 1)

A methanolic solution (10 ml) of Ni(CH₃COO)₂·4H₂O (0.24 g, 1.0 mmol) was added to L in methanol (0.46 g, 1.0 mmol). Continued stirring of the mixture for 1 h at room temperature resulted in a brick-red precipitate, which was filtered and washed with methanol followed by diethyl ether and dried in a desiccator containing anhydrous CaCl₂. Yield 81%; red-coloured solid; m.p. 281 °C. Anal. for C₂₈H₂₈N₂NiO₄ (%): found (calcd): C, 65.25 (65.27); H, 5.45 (5.48); N, 5.43 (5.44). UV–visible (CH₃CN, λ_{max},



SCHEME 1 Synthesis of metal complexes 1–4

nm): 272, 315, 375, 542. FT-IR (KBr, ν , cm^{-1}): 3201 ($-\text{C}\equiv\text{C}-\text{H}$), 2929 (asymmetric $-\text{C}-\text{H}$), 2845 (symmetric $-\text{C}-\text{H}$), 2109 ($-\text{C}\equiv\text{C}-$), 1591 ($-\text{C}=\text{N}$). ESI-MS (m/z): 515.21.

2.2.4 | Synthesis of complex 3 (Scheme 1)

A methanolic solution (10 ml) of $\text{Zn}(\text{O}_2\text{CCH}_3)_2(\text{H}_2\text{O})_2$ (0.136 g, 1.0 mmol) was added to L in methanol (0.46 g, 1.0 mmol) with constant stirring for 3 h at room temperature. The pale yellow precipitate obtained was filtered and washed with cold methanol followed by diethyl ether and dried in a desiccator containing anhydrous CaCl_2 . Yield 74%; white solid; m.p. 276 °C. Anal. for $\text{C}_{28}\text{H}_{28}\text{N}_2\text{O}_4\text{Zn}$ (%): found (calcd): C, 64.41 (64.44); H, 5.39 (5.41); N, 5.34 (5.37). UV-visible (CH_3CN , λ_{max} , nm): 288, 314, 381. FT-IR (KBr, ν , cm^{-1}): 3199 ($-\text{C}\equiv\text{C}-\text{H}$), 2934 (asymmetric $-\text{C}-\text{H}$), 2850 (symmetric $-\text{C}-\text{H}$), 2114 ($-\text{C}\equiv\text{C}-$), 1599 ($-\text{C}=\text{N}$). ESI-MS (m/z): 543.21.

2.2.5 | Synthesis of complex 4 (Scheme 1)

A methanolic solution (10 ml) of VOSO_4 (0.164 g, 1.0 mmol) and triethylamine (2 mmol) was added dropwise to a hot methanolic solution of L (0.46 g, 1.0 mmol). The resulting solution was stirred for 1 h and then the mixture was further refluxed for 3 h. The dark green-coloured precipitate was

filtered and washed with cold methanol followed by diethyl ether and dried in a desiccator containing anhydrous CaCl_2 . Yield 83%; dark green-coloured solid; m.p. 289 °C. Anal. for $\text{C}_{28}\text{H}_{28}\text{N}_2\text{O}_5\text{V}$ (%): found (calcd): C, 64.21 (64.24); H, 5.37 (5.39); N, 5.32 (5.35). UV-visible (CH_3CN , λ_{max} , nm): 271, 351, 579. FT-IR (KBr, ν , cm^{-1}): 3195 ($-\text{C}\equiv\text{C}-\text{H}$), 2922 (asymmetric $-\text{C}-\text{H}$), 2847 (symmetric $-\text{C}-\text{H}$), 2110 ($-\text{C}\equiv\text{C}-$), 1589 ($-\text{C}=\text{N}$). ESI-MS (m/z): 524.12.

3 | RESULTS AND DISCUSSION

The synthesized compounds 1–4 are stable in both solid state and solution at room temperature. They are soluble in all the common organic solvents except methanol and ethanol. All four metal complexes were structurally characterized using various spectral techniques. The molar conductance values ($5\text{--}11 \Omega^{-1} \text{mol}^{-1} \text{cm}^2$) measured in dimethylsulfoxide (DMSO) indicate that 1–4 are non-electrolyte in nature. The molecular geometry of 1–4 derived from spectral techniques is supported by quantum mechanical studies.

3.1 | Density functional theory (DFT) studies

The molecular geometry of 1–4 was optimized at B3LYP/LANL2DZ levels in the gas phase using Gaussian 09 W

(Figure S1). The calculated bond lengths and bond angles are given in Tables S1 and S2.^[12] The B3LYP method with LANL2DZ basis set gives valuable metal–nitrogen bond distances and the molecular geometries of the complexes were predicted by calculating τ ($=(\beta - \alpha)/60$) values,^[13] where α and β are the equatorial and axial bond angles, respectively. For all the complexes, α (N(2)–Cu(1)–N(1), N(1)–Ni(1)–N(2), N(2)–Zn(1)–N(1) and N(1)–V(1)–N(2)) values are 86.01°, 86.95°, 88.98° and 93.58° and β (O(3)–Cu(1)–O(2), O(2)–Ni(1)–O(1), O(3)–Zn(1)–O(2) and O(3)–V(1)–O(2)) values are 90.11°, 91.12°, 91.58° and 105.10°, respectively. From these values the calculated τ values are 0.068, 0.069 and 0.043 for **1**, **2** and **3**, respectively, suggesting square planar geometry for the Cu(II), Ni(II) and Zn(II) centres.^[14] In the case of complex **4**, the value of τ is 0.21, which indicates a square pyramidal geometry for the oxovanadium(IV) centre.^[15]

Frontier molecular orbital analyses were carried out for all the complexes (Figures 1 and S2). The HOMO–LUMO energy gap values are used to predict the chemical reactivity and bioactivity of molecules.^[16] When a molecule has lower HOMO–LUMO energy gap this implies higher chemical reactivity and shows a significant degree of intramolecular charge transfer from the electron-donor groups to the electron-accepter groups. Molecules having high E_{HOMO} are excellent electron donors while those having low E_{LUMO} energy are excellent electron acceptors. A molecule having

higher HOMO–LUMO energy gap implies the stability of the molecule and lower reactivity in chemical reactions.^[17] The electronic properties of the molecules were determined from the total energies and the Koopman theorem. The ionization potential ($\text{IP} = -E_{\text{HOMO}}$) and electron affinity ($\text{EA} = -E_{\text{LUMO}}$) were calculated. Also, other important quantities such as electronegativity (χ), hardness (η), softness (ζ) and electrophilicity index (ψ) were determined from IP and EA values (Table S3). From the results it is clear that complex **1** has higher chemical reactivity when compared to the other complexes.

The Bader atoms in molecules method was used to explain the nature of the bonding in the metal complexes. The contour maps for complexes **1–4** show the presence of bond critical points (BCPs; blue dots) and ring critical points (orange dots; Figure S3). The Laplacian electron density $\nabla^2\rho(r) < 0$ indicates a covalent-type interaction, while $\nabla^2\rho(r) > 0$ indicates an ionic or closed-shell type of interaction.^[18] The smallest $\nabla^2\rho(r)$ and $H(r)$ and largest $\delta(\text{M–L})$ values indicate that the M–N bonds are covalent in character. The $\nabla^2\rho(r)$ and $H(r)$ values at the BCPs reveal that the M–O bonds are ionic in character. The ellipticity values demonstrate that the M–N bonds of all complexes are in the range 0.014–0.208 and the bond stability order is **1** > **3** > **2** > **4**. The results reveal that all the M–L bonds are partially ionic and covalent in character demonstrated by low $\rho(r)$, positive $\nabla^2\rho(r)$ and negative $H(r)$ values (Table S4). This type of

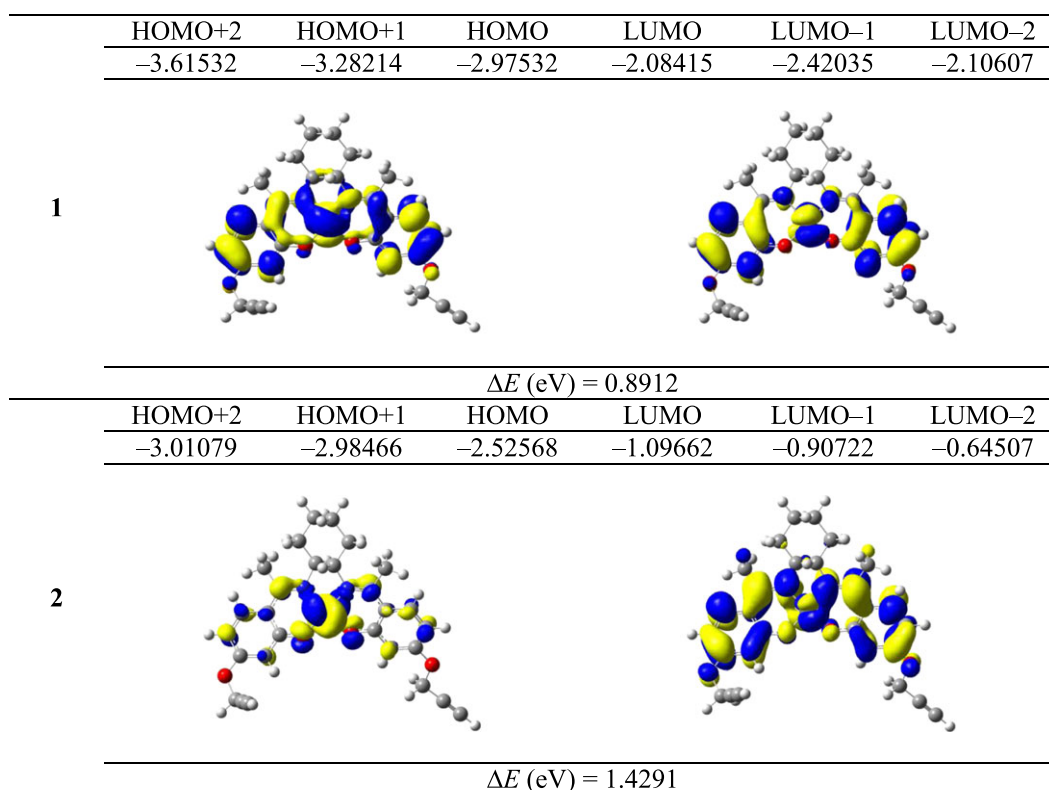


FIGURE 1 Frontier molecular orbital diagrams of complexes **1** and **2**

bonding character has been explained as 'transit closed shell' bonding with some covalent interactions.^[19]

3.2 | Spectroscopy

In the FT-IR spectrum of L, the stretching frequencies of phenolic hydroxyl (Ar—O) around 3269–3441 cm^{-1} and azomethine (—C=N—) at 1604 cm^{-1} are shifted to lower values in the spectra of the complexes indicating the coordination of hydroxyl oxygen atom and azomethine nitrogen to metal ion (Figure S4). All the metal complexes exhibit bands in the range 560–640 and 495–510 cm^{-1} , assigned as (M—O) and (M—N),^[12] indicating that the phenolic oxygen and azomethine nitrogen atoms are coordinated with metal ion. The V=O stretching frequency is observed at 1035 and 1039 cm^{-1} showing that the green-coloured vanadium complex has a square pyramidal structure.^[12]

Electronic absorption spectra of **1–4** were recorded in acetonitrile solution at room temperature. The complexes show two bands in the range 271–282 and 351–382 nm corresponding to intraligand transitions. The broad band appearing in the region 563 nm (**1**, $^1A_{1g} \rightarrow ^1B_{1g}$), 542 nm (**2**, $^1A_{1g} \rightarrow ^1B_{2g}$) and 579 nm (**4**, $^2B_2 \rightarrow ^2B_1$) corresponds to d–d transition (Figure S5). The nature of the transitions in the electronic absorption spectra of **1–4** has been explained by time-dependent DFT theory at B3LYP/6-311G(d,p) level. All the metal complexes exhibit a high-energy absorption band in the range 200–385 nm which can be attributed to the ligand-to-metal or metal-to-ligand charge transfer transitions. The spectra show one lowest energy absorption band in the range 542–579 nm which can be attributed to the d–d transition (Table S5). The calculated values are in reasonable agreement with experimental values.

The X-band EPR spectra of complexes **1** and **4** in acetonitrile (10^{-3} M) were recorded at room temperature as well as at liquid nitrogen temperature using DPPH \cdot as internal standard. At room temperature, the EPR spectrum of complex **1** consists of a weak shoulder at $g_{\parallel} = 2.15$ and an intense signal at $g_{\perp} = 2.04$ having a typical derivative line shape. These are well-known features in the EPR spectra of mainly mononuclear Cu(II) complexes ($S = 1/2$). The observed g values ($g_{\parallel} > g_{\perp} > 2.00$) for the complex suggest that the unpaired electron in the Cu(II) ion is in the $d_{x^2-y^2}$ orbital.^[20] Therefore, a square-based geometry around the Cu(II) is expected in complex **1**. The hyperfine structure due to ^{63}Cu having a nuclear spin ($I = 3/2$) is not observed, possibly due to a strong spin–spin interaction characteristic of paramagnetic salts. To reduce the broadening of the signal in complex **1** and to determine the hyperfine interactions and superhyperfine interactions if any, the EPR spectrum of **1** was recorded in acetonitrile at 77 K (Figure S6). The EPR spectrum is axially symmetric with parallel component

($g_{\parallel} = 2.24$) and a strong perpendicular component ($g_{\perp} = 2.11$). The hyperfine structure is observed only in the parallel component due to the interaction of unpaired electrons of Cu(II) with $^{63,65}\text{Cu}$ having nuclear spin $I = 3/2$. The square planar complex $G = 2.41$ for complex **1** indicates that the ligand is strong field and the metal–ligand bonding in the complex is covalent. The EPR spectrum of the vanadium complex (**4**) shows a hyperfine splitting consistent with axial-type spectra of monomeric metal-bound species with d_{xy} ground-state configuration. The spectrum displays well-resolved ^{51}V ($I = 7/2$) hyperfine lines and spin Hamiltonian parameters $g_x, g_y = 1.95, g_z = 1.93, A_x, A_y = 59.5 \times 10^{-4} \text{ cm}^{-1}$ and $A_z = 165.7 \times 10^{-4} \text{ cm}^{-1}$ indicate the presence of mononuclear V(IV) moiety in the complex.

3.3 | Stability of complexes

The stability of synthesized complexes in aqueous solution was measured over different time intervals of 24, 48 and 72 h using a scanning kinetic program with a UV–visible spectrophotometer (Figure S7). The absorption spectra of **1–4** recorded directly after dilution do not show any differences after 24, 48 and 72 h, demonstrating the stability of the complexes in solution.

3.4 | Catechol oxidation studies

Catecholase-like activity of complexes **1–4** was evaluated at 25 °C in aerobic condition spectrophotometrically by monitoring the oxidation of 3,5-DTBC in acetonitrile at *ca* 400 nm as a function of time. The acetonitrile solutions of complexes (10^{-4} M) were treated with 100 eq. of 3,5-DTBC. After the addition of substrate a new band appears at 405 nm with time due to the formation of the oxidized product 3,5-di-*tert*-butylquinone (3,5-DTBQ) (Figures 2 and S8). The spectra of all the complexes show marked changes immediately after the addition of 3,5-DTBC. The product 3,5-DTBQ was purified by column chromatography using a hexane–ethyl acetate eluent mixture and characterized using ^1H NMR, ^{13}C NMR and ESI-MS (Figure S9). Yield 72%; white solid; m.p. 112 °C. Anal. for $\text{C}_{14}\text{H}_{20}\text{O}_2$ (%): found (calcd): C, 76.31 (76.33); H, 9.14 (9.15). ^1H NMR (CDCl_3 , 400 MHz, δ , ppm): 1.31 (s, 9 H), 1.48 (s, 9 H), 6.58 (d, 1 H), 6.74 (d, 1 H). ^{13}C NMR (CDCl_3 , 400 MHz, δ , ppm): 28.94 (C10), 32.08 (C9), 35.47 (C5), 35.62 (C8), 111.03 (C3), 115.21 (C6), 137.55 (C7), 138.36 (4), 139.87 (C1), 139.82 (C2). ESI-MS (m/z): 238.26 (100%) [3,5-DTBQ] + H_2O .

3.4.1 | Kinetic studies

The kinetic aspects of the complexes were evaluated by monitoring the increase in the product 3,5-DTBQ. The rate constant for catalyst–complex mixture was calculated from the

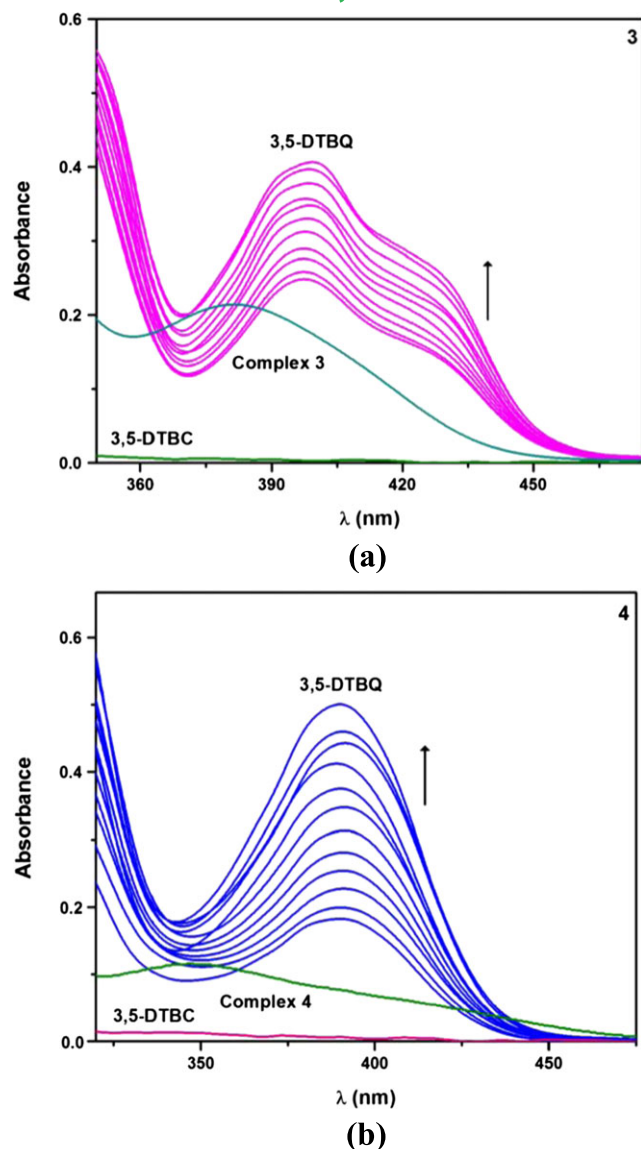


FIGURE 2 Catecholase activity by change in time-dependent spectral pattern of complexes (a) **3** and (b) **4** after addition of 3,5-DTBC in acetonitrile medium

$\log[A_{\alpha}/(A_{\alpha} - A_t)]$ versus time plot. In order to estimate the dependence of the rates on the substrate concentration, complexes were treated with various concentrations of 3,5-DTBC (10 to 100 eq.). At low concentrations of 3,5-DTBC, a first-order dependence on substrate concentration is observed; at higher concentrations of 3,5-DTBC, saturation kinetics are observed. The obtained rates versus concentration of substrate are analysed on the basis of the Michaelis–Menten approach of enzymatic kinetics. The Michaelis–Menten constant (K_M) and maximum initial rate (V_{\max}) were calculated by linearization using Lineweaver–Burk plots (Figure S10).^[21] The K_{cat} values can be calculated by dividing the V_{\max} values by the concentration of the corresponding complexes. The turnover number values (k_{cat}) are given in Table 1 and the order is

TABLE 1 Kinetic parameters for oxidation of 3,5-DTBC catalysed by complexes **1–4**

Catalyst	V_{\max} (M s^{-1})	K_M (M)	Std error	k_{cat} (h^{-1})
1	2.50×10^{-3}	9.20×10^{-3}	6.20×10^{-4}	150.00
2	3.10×10^{-3}	1.01×10^{-4}	2.19×10^{-3}	186.00
3	1.70×10^{-3}	1.00×10^{-4}	4.05×10^{-3}	102.00
4	1.20×10^{-3}	2.00×10^{-4}	3.27×10^{-3}	72.00

$2 > 1 > 3 > 4$. The results clearly indicate that complex **2** is more active than the other complexes.

3.4.2 | EPR titrations

In the catalytic reaction, organic radical and intermediate species are produced by the complexes. For that motivation, EPR spectra of complexes (10^{-3} M) were obtained after the addition of 3,5-DTBC (10^{-1} M) in acetonitrile at room temperature at various time intervals (within 30 min). The free ligand and 3,5-DTBC mixture is EPR-silent under the experimental conditions. This implies that the oxidation reaction of 3,5-DTBC is occurring via a radical pathway only when complexes are used as catalyst. The EPR spectrum of complex **1** exhibits a weak signal at $g \sim 2$ (free electron^[22] $g = 2.0023$) which is characteristic of the formation of organic radical species as the reaction intermediate in the catalytic process (Figures 3 and S11).^[23] The nickel and zinc salts are EPR-silent, whereas a weak signal at $g \sim 2$ is produced when the spectra are taken after the addition of 3,5-DTBC to complexes **2** and **3**, which indicates the formation of ligand-centred radical species and the radical formation is responsible for that oxidation. For complex **4**, a signal at $g \sim 1.988$ is attributed to the formation of organic radical species as the reaction intermediate in the catalytic process.

3.4.3 | ESI-MS study

To determine the complex–substrate intermediate and mechanistic inference of catecholase activity during the oxidation reaction, we recorded ESI-MS of the complexes and 1:100 mixture of the complexes and 3,5-DTBC within 5 min of mixing in acetonitrile solvent medium.

Complex **1** exhibits a base peak at $m/z = 537.22$ (100%), which can be assigned to the ‘ligand complex’ $[\mathbf{1}]\text{H}_2\text{O}$ (Figure S12a). After the addition of 3,5-DTBC to **1**, strong changes are observed in the spectrum: the two peaks at $m/z = 221.18$ and 243.31 can be assigned to the protonated quinone $[(3,5\text{-DTBQ})\text{H}^+]$ and the quinone–sodium aggregate $[(3,5\text{-DTBQ})\text{Na}^+]$, respectively. The peak at $m/z = 757.32$ corresponds to the monocationic species $[\mathbf{1}(3,5\text{-DTBC})]\text{H}_2\text{O}$ (Scheme S1 and Figure S13a). Complex **2** shows a base peak at $m/z = 515.21$ (100%), which can be assigned to the

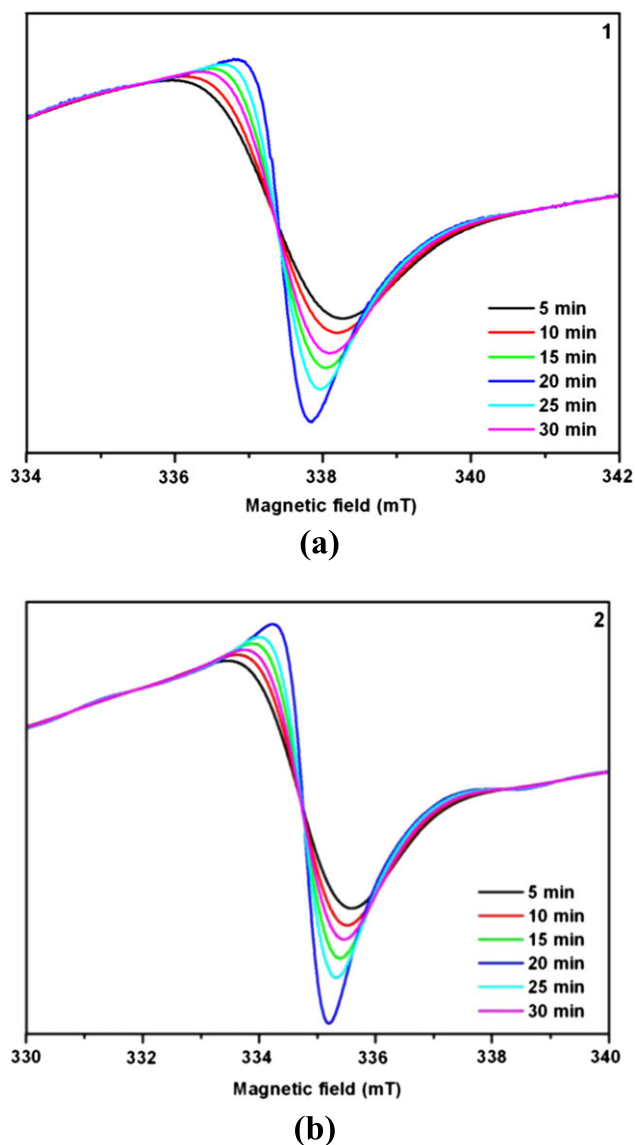


FIGURE 3 EPR spectra for different time intervals of acetonitrile solution of complexes (a) **1** and (b) **2** after the addition of 3,5-DTBC

'ligand complex' $[2]H^+$ (Figure S12b). After the addition of 3,5-DTBC to **2**, significant changes are observed in the spectrum: the two peaks at $m/z = 221.54$ and 243.22 can be assigned to the protonated quinone $[(3,5-DTBQ)]H^+$ and the quinone-sodium aggregate $[(3,5-DTBQ)]Na^+$, respectively. The peak at $m/z = 735.31$ corresponds to the monocationic species $[2(3,5-DTBC)]H^+$ (Figure S13b). Complex **3** exhibits a base peak at $m/z = 543.21$ (100%), which can be assigned to the 'ligand complex' $[3]Na^+$ (Figure S12c). After the addition of 3,5-DTBC to complex **1**, marked changes are observed in the spectrum: the two peaks at $m/z = 221.21$ and 243.35 can be assigned to the protonated quinone $[(3,5-DTBQ)]H^+$ and the quinone-sodium aggregate $[(3,5-DTBQ)]Na^+$, respectively. The peak at $m/z = 758.02$ corresponds to the monocationic species $[3(3,5-DTBC)]H_2O$ (Scheme S1 and Figure S13c). Complex **4** exhibits a

base peak at $m/z = 524.12$ (100%), which can be assigned to the 'ligand complex' $[4]H^+$ (Figure S12d). After the addition of 3,5-DTBC to **4**, marked changes are observed in the spectrum: the two peaks at $m/z = 221.05$ and 243.21 can be assigned to the protonated quinone $[(3,5-DTBQ)]H^+$ and the quinone-sodium aggregate $[(3,5-DTBQ)]Na^+$, respectively. The peak at $m/z = 766.21$ corresponds to the monocationic species $[4(3,5-DTBC)]Na^+$ (Figure S13d).

The spectral results reveal the formation of catalyst-substrate as intermediates which take part in substrate activation during the oxidation of 3,5-DTBC to 3,5-DTBQ in the presence of oxygen. After the quinone molecule is released, the catalyst is regenerated and the catalytic cycle is continued. The oxygen that takes part in this process is converted to H_2O_2 . In general, for the reported generalized catecholase reaction mechanism,^[23] electron transfer is mainly facilitated by the metal centre and then further delocalized via $-C=N$ bond of metal Schiff base complex to the adjacent conjugate system.

3.4.4 | Electrochemical study

Electrochemical properties of complexes **1–4** were investigated using cyclic voltammetry in acetonitrile solution containing 0.1 M TBAP as the supporting electrolyte in the potential range -1.2 to $+1.2$ V versus Ag/Ag^+ reference electrode at room temperature. Cyclic voltammograms of **1–4** are shown in Figure S14. An irreversible oxidation peak is observed for **1** at E_{pa} values of -0.32 and 0.58 V and is probably due to Cu^0/Cu^I and Cu^{II}/Cu^{III} . A quasi-reversible couple is observed at 0.11 V (E_{pa}) and -0.34 V (E_{pc}) due to Cu^I/Cu^{II} and Cu^{II}/Cu^I . Upon the addition of 3,5-DTBC to complex **1**, the irreversible oxidative wave is replaced by new peaks at -0.38 and 0.63 V. The quasi-reversible couple is replaced by a new couple at 0.20 and -0.39 V. From the results, the anodic peak at 0.16 V represents the oxidation of Cu^{II} -bound 3,5-DTBC to free 3,5-DTBQ and the cathodic peak at -0.38 V represents the reduction of free 3,5-DTBQ to Cu^{II} -bound deprotonated 3,5-DTBC. For complex **2**, a cathodic wave at $ca - 1.0$ V corresponds to the reduction of Ni^{II}/Ni^I . In addition, the complex displays two anodic waves at $ca + 0.62$ and $ca + 0.95$ V. The former oxidation peak corresponds to the oxidation of Ni^{II}/Ni^{III} and the latter to the reduction of the $-C=N$ bond. After the addition of 3,5-DTBC to the complex, the cathodic wave at $ca - 1.0$ V is shifted to $ca - 0.98$ V and the oxidation peaks at $ca + 0.62$ and $+0.95$ V are shifted to $ca + 0.65$ and $+0.98$ V. These results show that the variation in the oxidation state of the metal complexes is due to complex-3,5-DTBC aggregation.^[24] For complex **3**, the oxidation state may undergo change from $+2$ to the rare low-valent $+1$ state.^[25] Since Zn^{II} is redox innocent, the process is attributable to reduction of the ligand backbone, most likely with formation of an imine

radical, as reported by other groups with similar systems,^[26] and shows irreversible reduction peaks at -0.11 to -0.85 V. After the addition of 3,5-DTBC to the complex, two irreversible reduction peaks are slightly shifted due to the aggregation of complex and substrate. Complex **4** exhibits a reversible peak at *ca* 0.46 V and an irreversible peak in the region -0.91 to -1.0 V in acetonitrile solvent. The peak at *ca* 0.46 V is due to the $[\text{V}^{\text{VO}}(\text{L}^1)]^+ / [\text{V}^{\text{IV}}\text{O}(\text{L}^1)]$ redox process.^[27] However the reductive process $[\text{V}^{\text{IV}}\text{O}(\text{salen})] / [\text{V}^{\text{III}}\text{O}(\text{salen})]^-$ has not been reported for related $(\text{VO})^{2+}(\text{salen})$ complexes, but these types of redox couples were reported in various vanadium complexes.^[27] Upon the addition of 3,5-DTBC to the complex, the reversible reaction peak and irreversible reaction peaks are slightly shifted due to complex–substrate aggregation.

3.4.5 | Detection of d–d transition band in catalytic reactions

Time-dependent electronic spectra of complexes **1**, **2** and **4** were recorded in the range 500–900 nm after mixing of metal complex with 3,5-DTBC. After the addition of complex **1** to 3,5-DTBC the d–d band intensity decreases (Figure S15a) indicating an electron transfer process from catechol to the Cu(II) centre which is consequently reduced to Cu(I).^[28] Also, the d–d transition band intensities of complexes **2** and **4** are decreased (Figure S15b,c) indicating that the coordination numbers of Ni(II) and V(IV) change during development of complex–substrate aggregate.^[29]

3.5 | Hydrolysis of Phosphomonoester

To study the phosphatase activity of complexes **1–4**, 4-NPP was used as a substrate. Their hydrolytic activity was examined spectrophotometrically by monitoring the time evolution of *p*-nitrophenolate at 425 nm in acetonitrile. The spectral changes of the complexes are shown in Figures 4 and S16.

3.5.1 | Kinetic studies

Kinetic studies of the complexes were conducted using the initial rate method by monitoring the rate of increase in the intensity of the absorption band at *ca* 423 nm, which corresponds to an increase in *p*-nitrophenolate concentration. First-order kinetics are observed at lower concentration which slowly differs from unity at higher concentration and finally attains a saturation curve. K_M , V_{max} and k_{cat} were determined from plots of $1/V$ versus $1/[\text{S}]$, known as Lineweaver–Burk plots (Figure S17). All the parameters are given in Table 2. The catalytic activity of the metal complexes follows the order $4 > 1 > 3 > 2$.

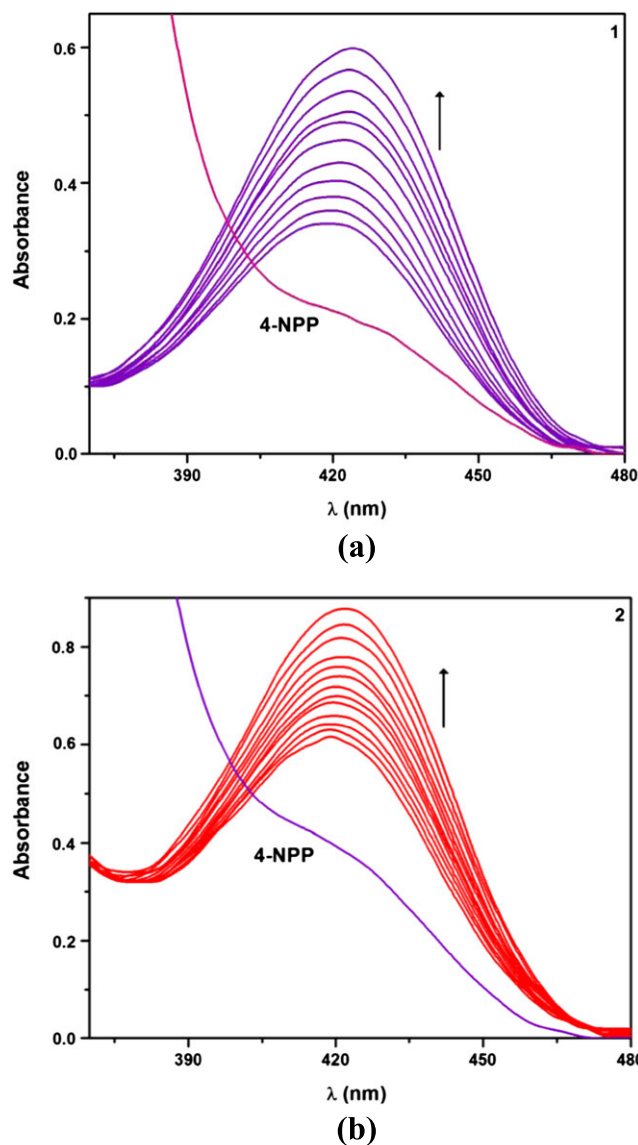


FIGURE 4 Hydrolysis of 4-NPP in the absence and presence of metal complexes (a) **1** and (b) **2** in acetonitrile medium

3.6 | DNA binding experiments

3.6.1 | Electronic absorption titration

UV–visible absorption spectroscopy is an efficient and widely employed method to determine the binding mode of metal complexes to DNA. In general, hyperchromism

TABLE 2 Kinetic parameters for phosphatase activity of complexes **1–4**

Catalyst	V_{max} (M s^{-1})	K_M (M)	Std error	k_{cat} (h^{-1})
1	1.90×10^{-3}	8.80×10^{-3}	4.11×10^{-4}	114.00
2	1.60×10^{-3}	1.14×10^{-3}	3.57×10^{-4}	96.00
3	1.70×10^{-3}	3.80×10^{-3}	2.32×10^{-3}	102.00
4	2.30×10^{-3}	6.60×10^{-3}	2.15×10^{-3}	138.00

and hypochromism are the spectral features of DNA indicating modification of its double helix structure. The extent of shift and hypochromism can be observed with the intercalative interaction of the complexes to DNA connecting a stacking interaction between aromatic chromophore and the base pairs of DNA.^[30] Upon the addition of DNA to the complexes, the absorption bands of the complexes are decreased (hypochromism) with a red shift of about 2 nm, which may be attributed to the intercalation between the aromatic conjugation and the stacking base pairs of DNA.^[31] The intrinsic binding constant, K_b , was determined using the following equation:

$$\frac{[\text{DNA}]}{\varepsilon_a - \varepsilon_f} = \frac{[\text{DNA}]}{\varepsilon_b - \varepsilon_f} + \frac{1}{K_b(\varepsilon_a - \varepsilon_f)}$$

where [DNA] is the concentration of DNA in base pairs and ε_a , ε_f and ε_b are the apparent absorption coefficient corresponding to $A_{\text{obs}}/[\text{compound}]$, the extinction coefficient of the free compound and the extinction coefficient of the compound when fully bound to DNA. A plot of $[\text{DNA}]/(\varepsilon_a - \varepsilon_f)$ versus [DNA] gives a slope and intercept which are equal to $1/(\varepsilon_b - \varepsilon_f)$ and $1/K_b(\varepsilon_b - \varepsilon_f)$, respectively; K_b is the ratio of the slope to the intercept. K_b values are listed in Table 3 and are compared with those of similar types of compounds (Table S6). From the resulting values, all the metal complexes show similar binding affinity towards DNA due to the chelation of metal with ligand. The titration curves for the complexes in the absence and presence of DNA at various concentrations and plots of $[\text{DNA}]/(\varepsilon_a - \varepsilon_f)$ versus [DNA] for ligands and complexes with DNA are shown in Figures 5 and S18.

3.6.2 | Fluorescence studies

Fluorescence spectroscopy was used to investigate the binding interaction characteristics between chromophore and other compounds.^[32] Ethidium bromide (EB) is one of the most responsive fluorescent probes that binds to DNA through intercalation mode.^[33] In this method, the emission intensity of EB is decreased due to the displacement of EB from a DNA sequence by a quencher.^[34] The emission intensity decrease of EB at 605 nm (hypochromism) upon increasing the concentration of the complexes clearly shows that the

TABLE 3 DNA binding constant (K_b), stern–Volmer constant (K_q) and apparent binding constant (K_{app}) for complexes 1–4

Complex	K_b (M^{-1})	K_q (M^{-1})	K_{app} (M^{-1})
1	4.21×10^5	3.92×10^5	4.05×10^5
2	3.94×10^5	3.31×10^5	4.32×10^5
3	4.06×10^5	3.65×10^5	4.18×10^5
4	4.11×10^5	3.79×10^5	4.12×10^5

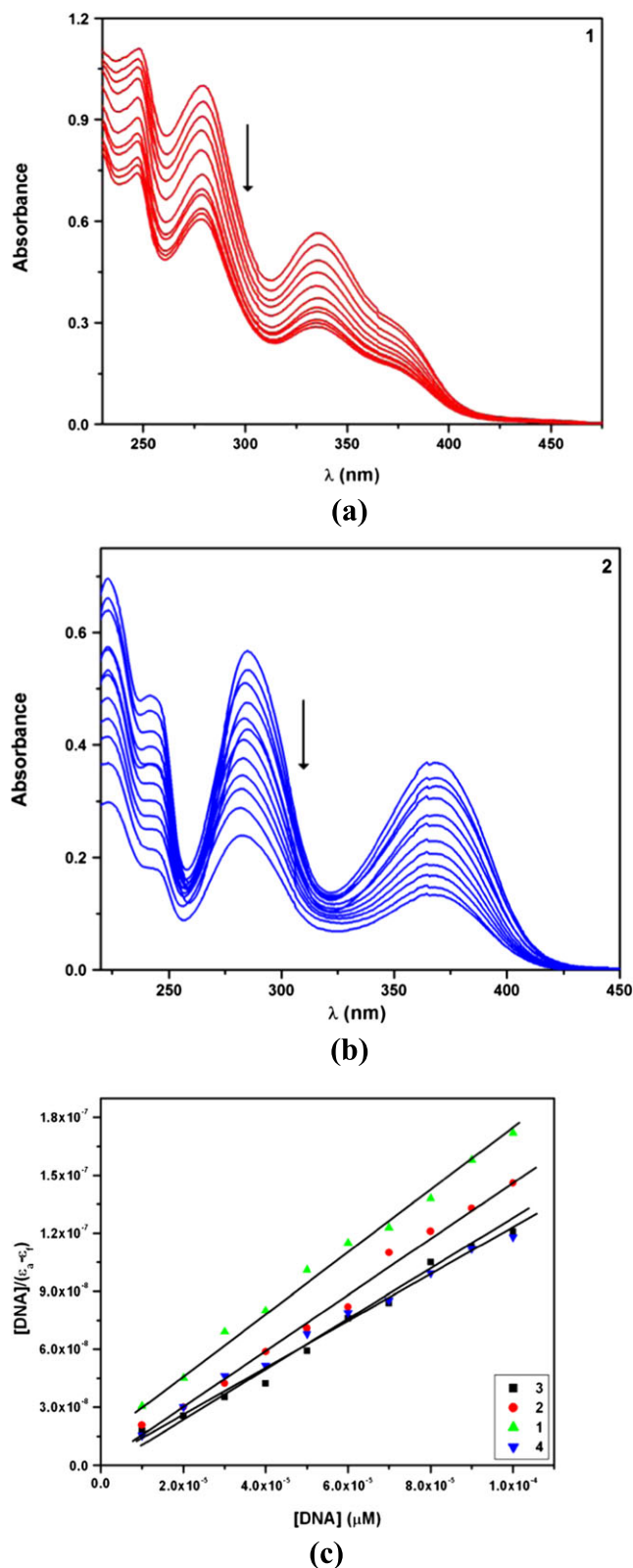


FIGURE 5 Electronic absorption spectra of complexes (a) 1 and (b) 2 in Tris-HCl buffer upon addition of CT-DNA. (c) plot of $[\text{DNA}]/(\varepsilon_a - \varepsilon_f)$ versus [DNA] for metal complexes with CT-DNA

EB molecules are displaced from their DNA binding sites by the complexes.^[35] The fluorescence quenching efficiency is calculated using the Stern–Volmer constant (K_{SV}) according to the classical Stern–Volmer equation:

$$\frac{F_0}{F} = 1 + K_q[Q]$$

where F_0 and F represent the fluorescence intensities of EB–DNA in the absence and presence of the complexes, $[Q]$ is the concentration of complexes and K_{SV} is a linear Stern–Volmer quenching constant obtained from the linear regression of F_0/F with $[Q]$. In the Stern–Volmer plots of F_0/F versus $[Q]$, the quenching constant (K_q) is given by the ratio of slope to intercept. The K_q values for the complexes are given in Table 3. Further, the apparent binding constant (K_{app}) was calculated using the equation

$$K_{app} = \frac{K_{EB}[EB]}{[complex]}$$

where [complex] is the concentration of the compound at which there is 50% reduction in the fluorescence intensity of EB, $K_{EB} = 1.0 \times 10^7 \text{ M}^{-1}$ and $[EB] = 2.5 \text{ }\mu\text{M}$.^[36] The binding constants and quenching constants of the complexes suggest that the interaction of the complexes with DNA should be via intercalation. All the spectroscopic studies suggest that the complexes can bind to DNA via an intercalative mode. The fluorescence quenching curves of EB bound to DNA in the presence of complexes and Stern–Volmer plots of fluorescence titrations of the complexes with CT-DNA are shown in Figures 6 and S19.

3.7 | DNA cleavage activity

The cleavage of supercoiled pUC19 DNA by complexes 1–4 was studied using various complex concentrations in the absence of external agents at pH = 7.2 (50 mM Tris–HCl/NaCl buffer at $25 \pm 0.5 \text{ }^\circ\text{C}$). All the complexes exhibit significant DNA cleavage with pUC19 DNA (Figure 7). As the concentration of the complexes is increased, supercoiled form of DNA (Form I) is gradually converted into nicked circular form (Form II) (lanes 2–6). Form I is completely converted into Form II when the concentration of complexes increases to $25 \text{ }\mu\text{M}$ (lane 6).

The cleavage mechanism of pUC19 DNA induced by complexes 1–4 was examined (Figure S20) and explained in the presence of singlet oxygen quencher L-histidine ($0.25 \text{ }\mu\text{M}$)^[37] (Figure S20a, lanes 2–5), superoxide dismutase (SOD; 4 units) (Figure S20a, lanes 6–9), EDTA as a chelating agent (Figure S20b, lanes 2–5) and hydroxyl radical scavenger DMSO (0.1 mM) (Figure S20b, lanes 6–9) under aerobic conditions.^[38] The mechanism of cleavage by complexes 1–4 is as follows: L-histidine, SOD and DMSO do not modify

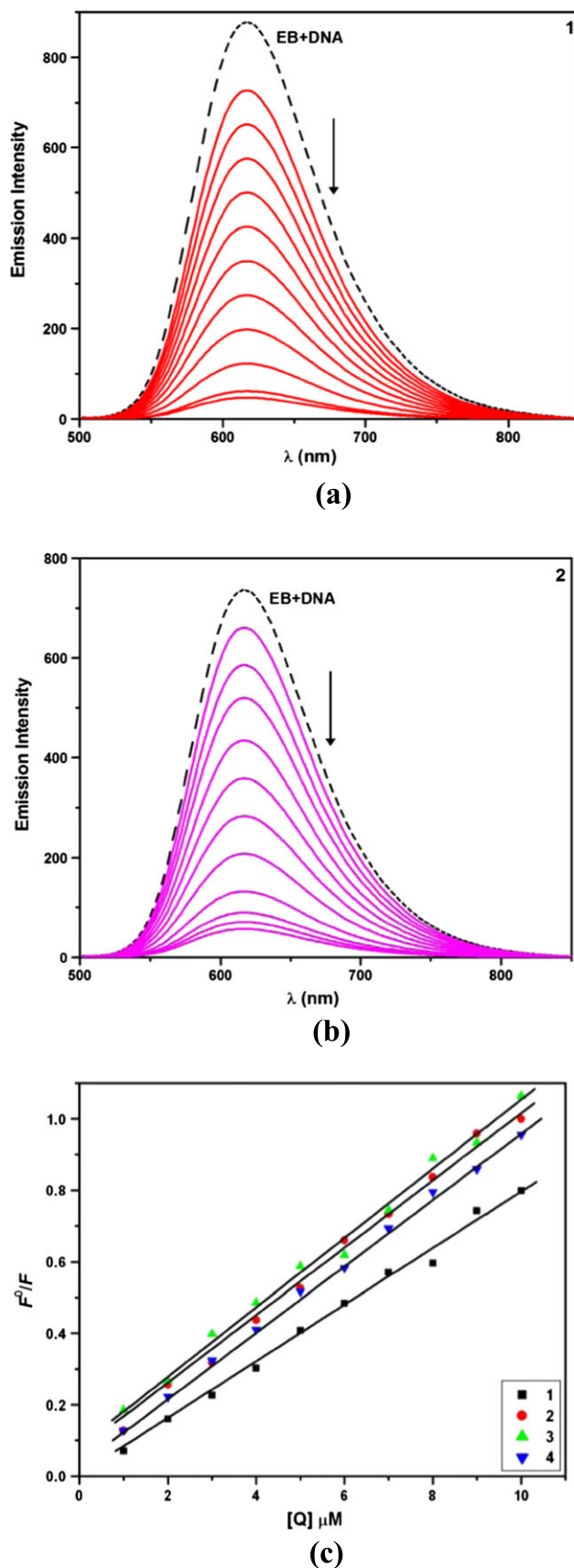


FIGURE 6 Fluorescence quenching curves of EB bound to DNA in the presence of complexes (a) 1 and (b) 2 in Tris–HCl buffer. (c) Stern–Volmer plots of metal complexes with CT-DNA

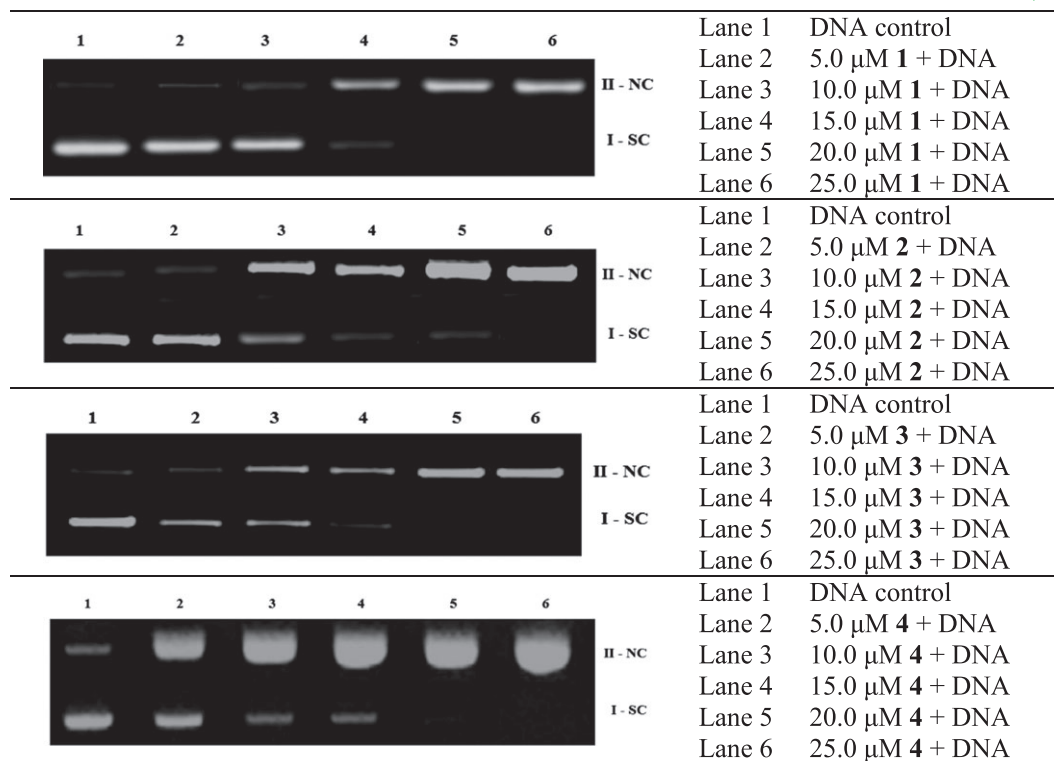


FIGURE 7 Agarose gel electrophoresis showing cleavage of pUC19 DNA incubated by **1–4** in Tris–HCl buffer

DNA cleavage activity and this rules out the possibility of cleavage by singlet oxygen, superoxide and hydroxyl radical. EDTA competently inhibits the DNA cleavage activity of the complexes in a way similar to that of nuclease (Figure S20b, lanes 2–5).^[39] These results show that the DNA cleavage by the complexes is via a hydrolytic pathway. To determine the hydrolytic nature of the cleavage mechanism, the nicked circular form of DNA was reacted with a T4 ligase enzyme. We observe the complete conversion of nicked form DNA to its original supercoiled form (Figure S21, lanes 6–9).^[40] The results reveal that all the complexes act as a synthetic nuclease, breaking the plasmid DNA via a hydrolytic mechanism.

3.8 | BSA protein binding studies

Electronic absorption titrations of BSA protein with complexes **1–4** were done to predict the type of quenching process. Addition of the complexes to the protein leads to an increase in the absorbance without changing the position of the absorption band (Figure S22). These results show that the type of interaction between complexes and protein is a static quenching process.^[41]

Emission spectra and Stern–Volmer plots of protein after addition of the complexes are shown in Figures 8 and S23. The protein solution (1.0×10^{-6} M) was titrated with various

concentrations of complexes (0–50 μM). The emission spectra of all the complexes were recorded in the wavelength range 290–450 nm upon excitation at 280 nm. The addition of complexes to the protein solution results in a significant decrease in the emission intensity at 340 nm. This observed hypochromicity indicates that the complexes interact hydrophobically with the BSA protein.^[42] The fluorescence quenching is described by the Stern–Volmer relation:

$$\frac{F_0}{F} = 1 + K_{SV}[Q]$$

where F_0 and F are the fluorescence intensities in the absence and presence of complexes. K_{SV} is a linear Stern–Volmer quenching constant and $[Q]$ is the concentration of complexes. K_{SV} can be calculated using a plot of (F_0/F) versus $[Q]$. When small molecules bind independently to a set of equivalent sites on a macromolecule, the equilibrium between free and bound molecules is demonstrated by the Scatchard equation^[43]

$$\log \frac{F_0 - F}{I} = \log K_b + n \log [Q]$$

where K_b is the binding constant of the complexes with BSA and n is the number of binding sites. From plots of $\log[(F_0 - F)/F]$ versus $\log[Q]$, K_b and n can be obtained (Figure S24). From the results it is clear that the metal

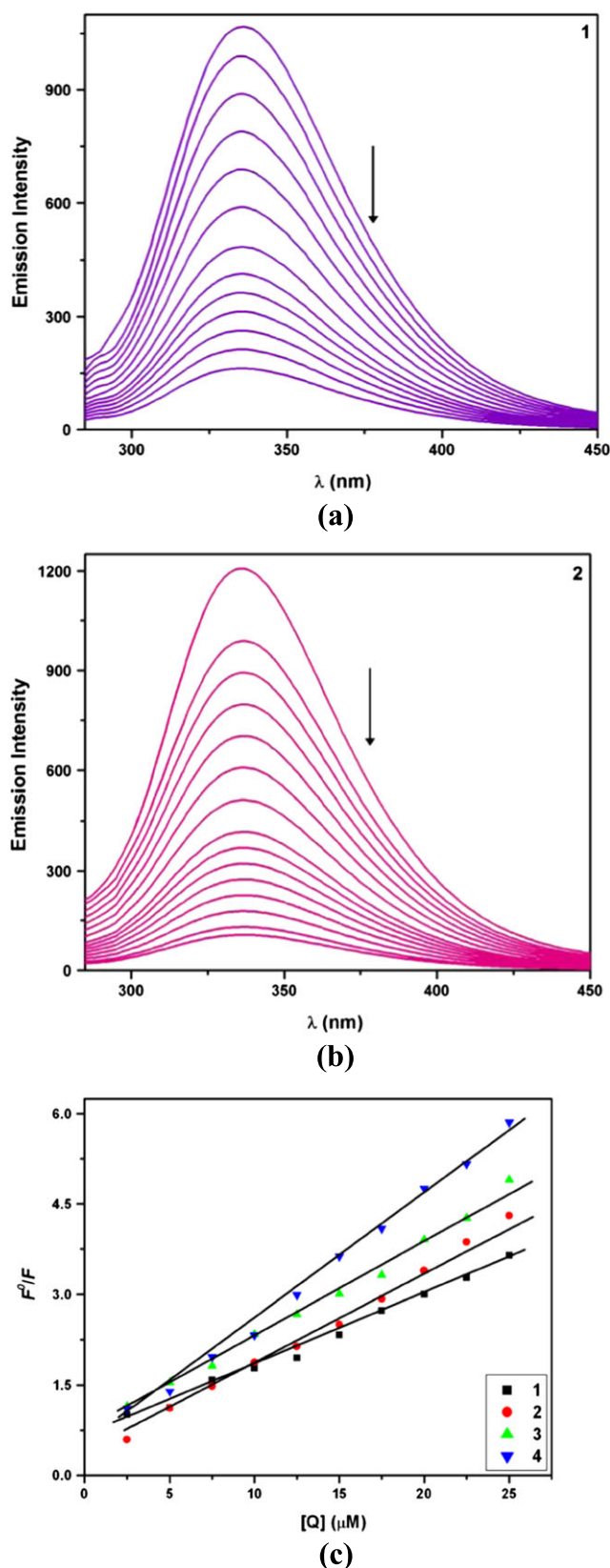


FIGURE 8 Fluorescence quenching spectra of BSA in the presence of increasing amounts of complexes (a) **1** and (b) **2** in Tris-HCl buffer. (c) stern-Volmer plots of complexes with BSA

complexes have only one binding site available to interact with BSA protein (Table 4).

3.9 | Cytotoxicity

The cytotoxic activity of metal complexes **1–4** was investigated against MCF7 and MIA-PA-CA-2 cells using the MTT assay (Figure S25). The IC_{50} values suggest that all the complexes have a significant inhibitory potency against proliferation of MCF7 ($\text{IC}_{50} = 14.9\text{--}22.2 \mu\text{mol l}^{-1}$) and MIA-PA-CA-2 ($\text{IC}_{50} = 94.4\text{--}97.8 \mu\text{mol l}^{-1}$) cell lines in a dose-dependent manner and are compared with similar types of compounds (Tables S7 and S8). This suggests that the metal complexes promote the interactions between complexes and cell DNA, which is absolutely a valuable factor for these metal complexes as promising candidates for new anti-tumour agents.

3.10 | Annexin V-Propidium iodide (PI) double staining

Annexin V-PI staining assay method was used to determine the mechanism of cell death caused by the metal complexes. This method clearly identifies the viable, apoptotic or necrotic population resulting after the treatment of metal complexes. MCF7 and MIA-PA-CA-2 cells (BT20) were treated with each metal complex for a period of 48 h. The untreated cells remain completely viable with no sign of apoptosis or necrosis. All the metal complexes induce cancer cell apoptosis and mostly in the early phase (Figure 9). These results are in agreement with the MTT results. The results clearly show that the cellular death triggered by the metal complexes follows the apoptosis pathway as reported earlier.^[44] The fluorescence imaging method was used to determine the effect of the metal complexes on the cancer cells. Bright field images were observed after the addition of metal complexes to the cancer cells due to cell death with alteration in the cellular morphology. Also, shrinking of the cells occurs followed by clustering and fragment formation. These results suggest that all the metal complexes mediated cell death taking place due to apoptosis, which is activated by fragmentation and damage of DNA.

TABLE 4 Protein binding constant (K_b), quenching constant (K_{SV}) and number of binding sites (n) for complexes **1–4**

Complex	K_b (M^{-1})	K_{SV} (M^{-1})	n
1	4.92×10^6	3.91×10^5	0.98
2	4.21×10^6	3.46×10^5	1.01
3	4.64×10^6	3.72×10^5	0.99
4	4.85×10^6	3.81×10^5	1.05

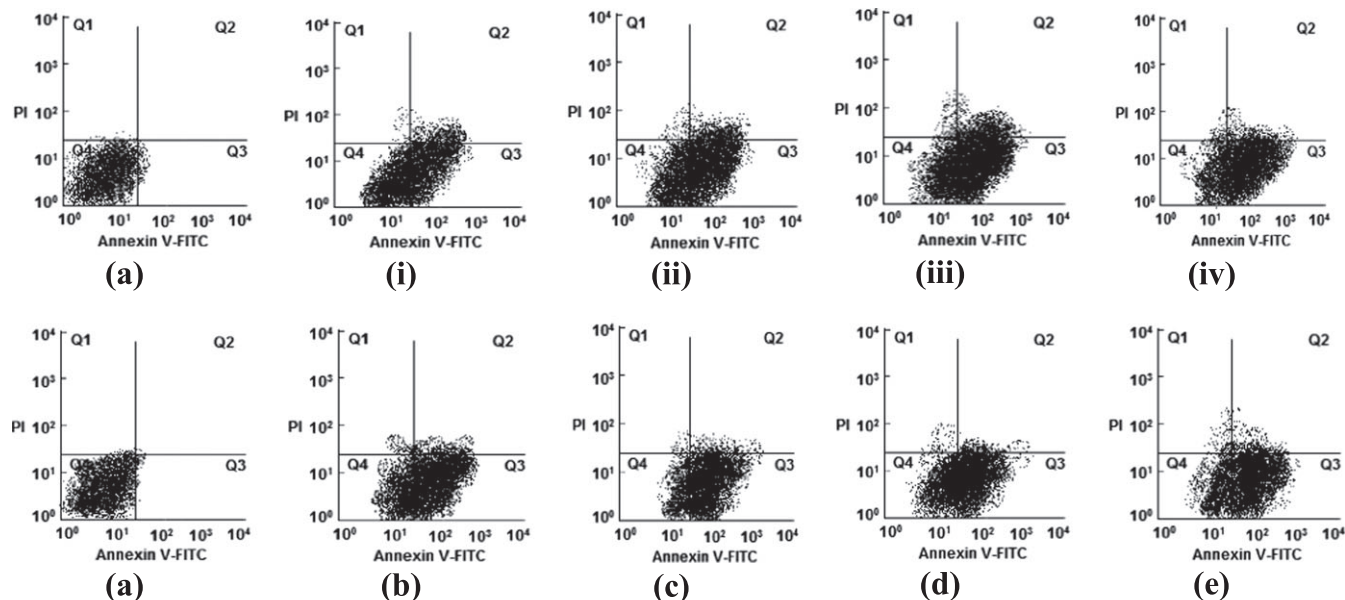


FIGURE 9 Apoptosis distribution of MCF7 cells (i–iv) and MIA-PA-CA-2 cells (b–e) after treatment with **1–4** ($10 \mu\text{mol l}^{-1}$) for 48 h. (a) control untreated cells; (b) cells treated with **1**; (c) cells treated with **2**; (d) cells treated with **3**; (e) cells treated with **4**. Q4: living cells; Q3: early apoptotic cells; Q2: late apoptotic cells; Q1: necrotic cells

3.11 | Comet assay

Single cell gel electrophoresis (comet assay) was used to determine whether the metal complexes induce DNA strand fragmentation, which is an indication of early apoptosis.^[45] MCF7 and MIA-PA-CA-2 cells were treated with the metal complexes, showing significant well-formed comets (Figures 10 and S26), whereas the control (untreated) cells show a round shape. The results reveal that all the metal complexes notably induce DNA damage and the length of the comet tail characterizes the extent of DNA fragmentation, which is further support for induction of apoptosis by the complexes.

3.12 | Computational studies

DFT analysis was carried out to determine the active species formed in the catalysis reaction. DFT calculations were done on the corresponding one-electron-reduced analogues **1**[−], **2**[−], **3**[−] and **4**[−] of the complexes at the B3LYP level using Gaussian 09 software. The one-electron-reduced monoanionic species **1**[−], **2**[−], **3**[−] and **4**[−] display a doublet ($S = 1/2$) ground state and the changes in the spin density visibly show a ligand-centred process for the reductive reaction (Figure S27). The results show one unpaired electron mainly localized in the C=N bond and carbon atoms of the aromatic

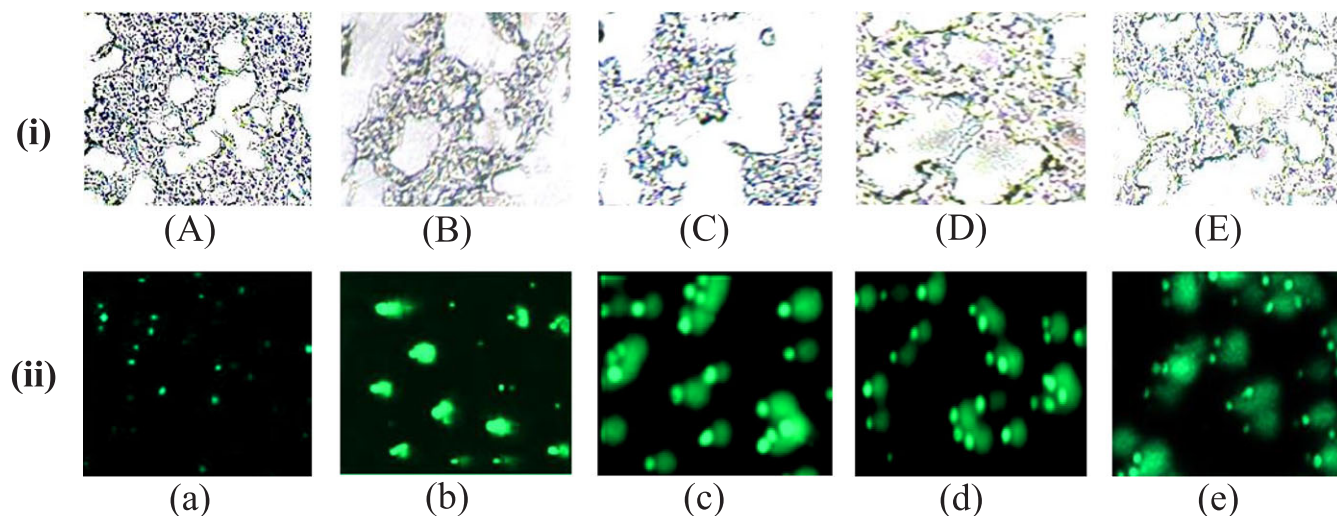


FIGURE 10 (i) cell morphology on treatment with metal complexes: (A–E) control and treatment with metal complexes **1–4**. (ii) induced DNA damage in MCF7 cancer cells treated with complexes and images of fragmentation detected by comet assay: (a–e) control and treatment with metal complexes **1–4**

ring and the other electron delocalized in the catechol ring and oxygen atoms. Therefore, the proposed electron transfer mechanism is supported by the orbital distribution in the complexes and the electron transfer is facilitated by the metal centre. The imine bond, —C=N , in the monoanionic species is significantly elongated (*ca* 0.024 Å), indicating the formation of imine radicals.

3.13 | Molecular docking studies

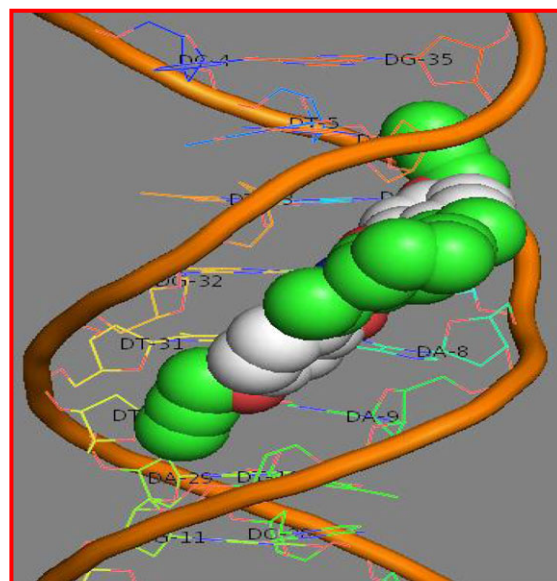
3.13.1 | Docking with DNA

Molecular docking is an extremely useful *in silico* computational tool for the rational design of chemotherapeutic drugs, which predicts non-covalent interaction between synthesized compounds and DNA nucleic acids. In our study, the synthesized complexes were subjected to molecular docking studies using the AutoDock Tools (ADT) version 1.5.6 and AutoDock vina docking programs. The conformation of docked complexes was analysed in terms of energy, hydrogen bonding and hydrophobic interaction between complexes and DNA. The binding free energy of the complexes was calculated from the docking scores. Details are given in Table S9.

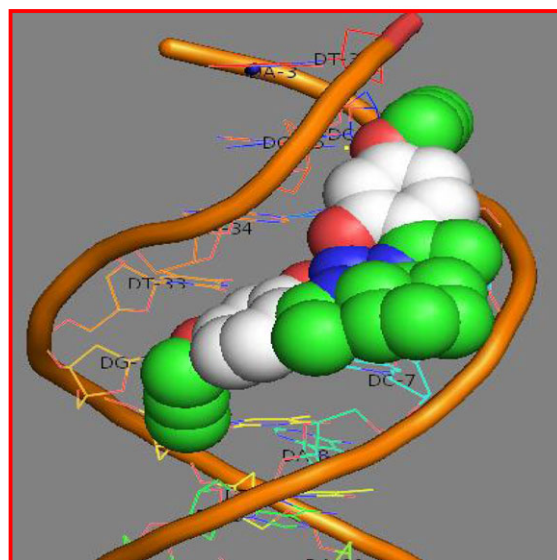
Molecular docking studies reveal that the docked complexes fit into the DNA comfortably involving van der Waals interactions, hydrophobic and hydrogen bonding contacts with DNA functional groups without disturbing the double helical structure of DNA, resulting in a binding energy between -10.2 and -12.5 kcal mol $^{-1}$. Complex 1 shows higher binding energy of -8.88 kcal mol $^{-1}$. The binding interactions of all the complexes with the B-DNA receptor are shown in Figures 11 and S28.

3.13.2 | Docking with BSA protein

In order to obtain insight into the favoured binding site location and binding mode, the molecular docking method was used to dock complexes 1–4 into BSA protein. Two principal binding sites, Trp134 and Trp213, are present in the BSA protein molecules,^[46] where Trp213 is placed within a hydrophobic binding pocket and Trp134 is located on the surface in the hydrophilic region of the molecule. Of the two binding sites, which one is favoured for a complex to bind can be analysed by docking complexes into the BSA protein using AutoDock vina. The docking results reveal that Trp134 is more preferential for the binding of the complexes than Trp213 (Table S9). Tryptophan quenching fluorescence studies reveal that all the complexes bind BSA protein through only one binding site. These spectroscopy results simultaneously with the molecular docking studies give a complete understanding of the BSA binding activities of the complexes, proving that all the complexes can strongly quench the intrinsic fluorescence of BSA through the static



1



2

FIGURE 11 Docking poses of complexes 1 and 2 with B-DNA (1BNA)

quenching mechanism with the ratio of the complex to BSA being 1:1, and the most probable binding site is Trp134. The binding interactions of complexes 1–4 with the BSA protein are shown in Figure S29.

4 | CONCLUSIONS

We have synthesized four mononuclear Cu(II), Ni(II), Zn(II) and V(IV) metal complexes and structurally characterized them using various spectral techniques. The catecholase-mimicking activity of the complexes was investigated and the results reveal that all the complexes have the ability to

oxidize 3,5-DTBC to 3,5-DTBQ in aerobic condition. ESI-MS studies were performed in the presence of 3,5-DTBC, explaining the possible complex–substrate intermediates. The X-band EPR spectral results indicate that the metal centres are involved in the catecholase activity. Ligand-centred radical generation was further confirmed by DFT calculation. The phosphatase (4-NPP) activity of the complexes was investigated and the results demonstrate that the compounds exhibit excellent activity in acetonitrile medium. The interactions of the complexes with CT-DNA and BSA protein were investigated using absorption and fluorescence titration methods. The studies reveal that all the complexes strongly interact with CT-DNA and BSA protein. The complexes exhibit significant hydrolytic cleavage of supercoiled pUC19 DNA. *In vitro* cytotoxicity results for the complexes towards MCF7 and MIA-PA-CA-2 cell lines demonstrate that they exhibit significant cytotoxic activity. The molecular docking technique was employed to determine the binding affinity of the complexes with DNA and protein molecules.

ACKNOWLEDGEMENTS

The financial support received from the Science and Engineering Research Board (SERB), Department of Science and Technology (DST), Government of India, New Delhi (EMR-II/2014/000081) and Board of Research in Nuclear Sciences (BRNS), DAE-BARC, Mumbai, India (no. 35/14/03/2014) is gratefully acknowledged. C.B. is grateful to CSIR, India for his fellowship. STIC, Cochin is acknowledged for performing the NMR analysis.

REFERENCES

- [1] a) W. Hong, H. Lee, T. H. Noh, O. S. Jung, *Dalton Trans.* **2013**, 42, 11092; b) J. Adhikary, A. Chakraborty, S. Dasgupta, S. K. Chattopadhyay, R. Kruszynski, A. T. Kruszynska, S. Stepanovic, M. G. Pavlovic, M. Swart, D. Das, *Dalton Trans.* **2016**, 45, 12409.
- [2] a) K. D. Karlin, Z. Tyeklar (Eds), *Bioinorganic Chemistry of Copper*, Chapman & Hall, New York **1993**; b) P. Halder, S. Paria, T. K. Paine, *Chem. – Eur. J.* **2012**, 18, 11778; c) S. Paria, P. Halder, T. K. Paine, *Angew. Chem. Int. Ed.* **2012**, 51, 6195.
- [3] a) A. Banerjee, S. Sarkar, D. Chopra, E. Colacio, K. K. Rajak, *Inorg. Chem.* **2008**, 47, 4023; b) D. Ghosh, R. Mukherjee, *Inorg. Chem.* **1998**, 37, 6597; c) M. Thirumavalavan, P. Akilan, M. Kandaswamy, K. Chinnakali, G. S. Kumar, H. K. Fun, *Inorg. Chem.* **2003**, 42, 3308; d) N. A. Rey, A. Neves, A. J. Bortoluzzi, C. T. Pich, H. Terenzi, *Inorg. Chem.* **2007**, 46, 348; e) A. Banerjee, R. Singh, E. Colacio, K. K. Rajak, *Eur. J. Inorg. Chem.* **2009**, 2, 277.
- [4] a) R. Sanyal, A. Guha, T. Ghosh, T. K. Mondal, E. Zangrando, D. Das, *Inorg. Chem.* **2014**, 53, 85; b) I. Majumder, P. Chakraborty, S. Das, H. Kara, S. K. Chattopadhyay, E. Zangrando, D. Das, *RSC Adv.* **2015**, 5, 51290; R. Sanyal, P. Chakraborty, E. Zangrando, D. Das, *Polyhedron* **2015**, 97, 55.
- [5] a) S. Delamey, M. Pascaly, P. K. Bhattacharya, K. Han, J. K. Barton, *Inorg. Chem.* **2002**, 41, 1966; b) Y. H. Liu, A. Li, J. Shao, X. Q. Song, C. Z. Xie, W. G. Bao, J. Y. Xu, *Dalton Trans.* **2016**, 45, 8036.
- [6] J. Qing, H. Daghiri, P. Beale, *J. Inorg. Biochem.* **2004**, 98, 1261.
- [7] a) R. P. Paitandi, R. K. Gupta, R. S. Singh, G. Sharma, B. Koch, D. S. Pandey, *Eur. J. Med. Chem.* **2014**, 84, 17; b) A. Lauria, R. Bonsignore, A. Terenzi, A. Spinello, F. Giannici, A. Longo, A. M. Almerico, G. Barone, *Dalton Trans.* **2014**, 43, 6108.
- [8] a) S. Bhattacharya, S. S. Mandal, *J. Chem. Soc., Chem. Commun.* **1995**, 2489; b) S. S. Mandal, U. Varshney, S. Bhattacharya, *Bioconjugate Chem.* **1997**, 8, 798; c) S. S. Mandal, N. V. Kumar, U. Varshney, S. Bhattacharya, *J. Inorg. Biochem.* **1996**, 63, 265; d) S. Routier, J. L. Bernier, J. P. Catteau, P. Colson, C. Houssier, C. Rivalle, E. Bisagni, C. Bailly, *Bioconjugate Chem.* **1997**, 8, 789; e) S. Routier, H. Vezin, E. Lamour, J. L. Bernier, J. P. Catteau, C. Bailly, *Nucleic Acids Res.* **1999**, 27, 4160; f) K. I. Ansari, J. D. Grant, G. A. Woldemariam, S. Kasiri, S. S. Mandal, *Org. Biomol. Chem.* **2009**, 7, 926; g) K. I. Ansari, S. Kasiri, J. D. Grant, S. S. Mandal, *Dalton Trans.* **2009**, 40, 8525.
- [9] a) O. Weinreb, T. Amit, O. Bar-Am, O. Chillag-Talmor, M. B. Youdim, *Ann. N. Y. Acad. Sci.* **2005**, 1053, 348; b) J. L. Kraus, B. Belleau, *Can. J. Chem.* **1975**, 53, 3141.
- [10] a) C. Balakrishnan, S. Natarajan, M. A. Neelakantan, *RSC Adv.* **2016**, 6, 102482; b) L. Subha, C. Balakrishnan, S. Thalamuthu, M. A. Neelakantan, *J. Coord. Chem.* **2015**, 68, 1021; P. J. K. Inba, B. Annaraj, S. Thalamuthu, M. A. Neelakantan, *Spectrochim. Acta A* **2013**, 104, 300.
- [11] a) V. Selvarani, B. Annaraj, M. A. Neelakantan, S. Sundaramoorthy, D. Velmurugan, *Spectrochim. Acta A* **2012**, 91, 329; b) C. Balakrishnan, L. Subha, M. A. Neelakantan, S. S. Mariappan, *Spectrochim. Acta A* **2015**, 150, 671.
- [12] a) V. Selvarani, B. Annaraj, M. A. Neelakantan, V. Silambarasan, D. Velmurugan, *Polyhedron* **2013**, 54, 74; b) D. L. Daughdrill, D. F. Martin, J. S. Binford Jr., *J. Inorg. Nucl. Chem.* **1970**, 32, 2885; c) N. S. Gwaram, H. Khaledi, H. Mohd Ali, *Acta Crystallogr E* **2013**, m813; d) M. Barwiolek, E. Szlyk, A. Surdykowski, A. Wojtczak, *Dalton Trans.* **2013**, 42, 11476; e) M. Barwiolek, E. Szlyk, T. M. Muziola, T. Lis, *Dalton Trans.* **2011**, 40, 11012; f) H. C. Lin, C. C. Huang, C. H. Shi, Y. H. Liao, C. C. Chen, Y. C. Lin, Y. H. Liu, *Dalton Trans.* **2007**, 781; g) M. J. Xie, L. Li, X. D. Yang, W. P. Liu, S. P. Yan, Y. F. Niu, Z. H. Meng, *Eur. J. Med. Chem.* **2010**, 45, 2327; h) P. Zabierowski, J. Szklarzewicz, R. Grybos, B. Modryl, W. Nitek, *Dalton Trans.* **2014**, 43, 17044.
- [13] R. C. Charles, K. M. G. Bush, S. P. Rowley, P. D. Boyle, *Inorg. Chem.* **1997**, 36, 6401.
- [14] U. M. Rafi, D. Mahendiran, A. K. Haleel, R. P. Nankar, M. Doble, A. K. Rahiman, *New J. Chem.* **2016**, 40, 2451.
- [15] M. M. Hanninen, A. Peuronen, P. Damlin, V. Tyystajarvi, H. Kivela, A. Lehtonen, *Dalton Trans.* **2014**, 43, 14022.
- [16] I. Fleming, *Frontier Orbitals and Organic Chemical Reactions*, John Wiley, New York **1976**.

- [17] P. Thanikaivelan, V. Subramanian, J. R. Rao, B. U. Nair, *Chem. Phys. Lett.* **2000**, 323, 59.
- [18] C. F. Matta, R. J. Boyd (Eds), *The Quantum Theory of Atoms in Molecules*, Wiley-VCH, Weinheim **2007** 1.
- [19] (a) E. Espinosa, I. Alkorta, J. Elguero, E. Molins, *J. Chem. Phys.* **2002**, 117, 5529; (b) M. Niskanen, P. Hirva, M. Haukka, *J. Chem. Theory Comput.* **2009**, 5, 1084; (c) S. K. Brayshaw, J. C. Green, G. K. Kohn, E. L. Sceats, A. S. Weller, *Angew. Chem. Int. Ed.* **2006**, 45, 452; (d) X. Li, J. Sun, Z. Sun, Y. Zeng, S. Zheng, L. Meng, *Organometallics* **2012**, 31, 6582; (e) J. A. Cabeza, J. F. Van der Maelen, S. G. Granda, *Organometallics* **2009**, 28, 3666.
- [20] D. Kivelson, R. Neiman, *J. Chem. Phys.* **1961**, 35, 149.
- [21] J. Adhikary, P. Chakraborty, S. Das, T. Chattopadhyay, A. Bauza, S. K. Chattopadhyay, B. Ghosh, F. A. Mautner, A. Frontera, D. Das, *Inorg. Chem.* **2013**, 52, 13442.
- [22] P. H. Rieger, *Electron Spin Resonance: Analysis and Interpretation*, Royal Society of Chemistry, Cambridge **2007**.
- [23] (a) A. Biswas, L. K. Das, M. G. B. Drew, G. Aromi, P. Gamez, A. Ghosh, *Inorg. Chem.* **2012**, 51, 7993; (b) A. Guha, T. Chattopadhyay, N. D. Paul, M. Mukherjee, S. Goswami, T. K. Mondal, E. Zangrando, D. Das, *Inorg. Chem.* **2012**, 51, 8750; (c) L. Benisvy, R. Wanke, M. F. C. G. D. Silva, A. J. L. Pombeiro, *Eur. J. Inorg. Chem.* **2011**, 2791.
- [24] T. Ghosh, J. Adhikary, P. Chakraborty, P. K. Sukul, M. S. Jana, T. K. Mondal, E. Zangrando, D. Das, *Dalton Trans.* **2014**, 43, 841.
- [25] (a) A. B. Mazaletskii, A. N. Zverev, V. G. Vinogradova, L. V. Alam, I. Y. Kvitko, *Zh. Obshch. Khim.* **1991**, 61, 2215; (b) H. Cox, C. Norris, G. Wu, J. Guan, S. Hessey, A. J. Stace, *Dalton Trans.* **2011**, 40, 11200; (c) T. Bollermann, C. Gemel, R. A. Fischer, *Coord. Chem. Rev.* **2012**, 256, 537.
- [26] (a) C. C. Lu, E. Bill, T. Weyhermuller, E. Bothe, K. Wieghardt, *J. Am. Chem. Soc.* **2008**, 130, 3181; (b) A. C. Bowman, C. Milsman, E. Bill, E. Lobkovsky, T. Weyhermuller, K. Wieghardt, P. Chirik, *J. Inorg. Chem.* **2010**, 49, 6110.
- [27] (a) K. Oyaizu, E. L. Dewi, E. Tsuchida, *Inorg. Chem.* **2003**, 42, 1070; (b) J. A. Bonadies, W. M. Butler, V. L. Pecoraro, C. J. Carrano, *Inorg. Chem.* **1987**, 26, 1218; (c) K. I. Smith, L. L. Borer, M. M. Olmstead, *Inorg. Chem.* **2003**, 42, 7410.
- [28] J. Mukherjee, R. Mukherjee, *Inorg. Chim. Acta* **2002**, 337, 429.
- [29] M. Das, R. Nasani, M. Saha, S. M. Mobina, S. Mukhopadhyay, *Dalton Trans.* **2015**, 44, 2299.
- [30] (a) S. A. Tysoe, A. D. Baker, T. C. Streckas, *J. Phys. Chem.* **1993**, 97, 1707; (b) J. M. Kelly, A. B. Tossi, D. J. McConnell, C. OhUigin, *Nucl. Acids Res.* **1985**, 13, 6017.
- [31] V. K. Verma, A. K. Asatkar, T. A. Jain, S. K. Tripathi, R. Singh, P. B. Hitchcock, S. Nigam, S. K. Gupta, *Polyhedron* **2009**, 28, 2591.
- [32] (a) N. Chitrapriya, S. T. Kamatchi, M. Zeller, H. Lee, K. Natarajan, *Spectrochim. Acta A* **2011**, 81, 128; (b) J. R. Lakowicz, G. Webber, *Biochemistry* **1973**, 12, 4161; (c) B. C. Baguley, M. Le Bret, *Biochemistry* **1984**, 23, 937.
- [33] (a) F. J. M. Almesa, D. Porschke, *Biochemistry* **1993**, 32, 4246; (b) B. D. Wang, Z. Y. Yang, Q. Wang, T. K. Cai, P. Crewdson, *Bioorg. Med. Chem.* **2006**, 14, 1880.
- [34] M. Alagesan, N. S. P. Bhuvanesh, N. Dharmaraj, *Dalton Trans.* **2013**, 42, 7210.
- [35] Y. B. Zeng, N. Yang, W. S. Liu, N. Tang, *J. Inorg. Biochem.* **2003**, 97, 258.
- [36] M. Lee, A. L. Rhodes, M. D. Wyatt, S. Forrow, J. A. Hartley, *Biochemistry* **1993**, 32, 4237.
- [37] H. Kishikawa, Y. P. Jiang, J. Goodisman, J. C. Dabrowiak, *J. Am. Chem. Soc.* **1991**, 113, 5434.
- [38] J. A. Cowan, *Curr. Opin. Chem. Biol.* **2001**, 5, 634.
- [39] J. Z. Wu, L. Yuan, J. F. Wu, *J. Inorg. Biochem.* **2005**, 99, 2211.
- [40] (a) A. Sreedhara, J. D. Cowan, *Chem. Commun.* **1737**, 1998; (b) S. Dhar, P. A. N. Reddy, A. R. Chakravarty, *Dalton Trans.* **2004**, 697.
- [41] D. S. Raja, N. S. P. Bhuvanesh, K. Natarajan, *Eur. J. Med. Chem.* **2011a**, 46, 4584.
- [42] D. S. Raja, G. Paramaguru, N. S. P. Bhuvanesh, J. H. Reibenspies, R. Renganathan, K. Natarajan, *Dalton Trans.* **2011b**, 40, 4548.
- [43] (a) M. R. Eftink, in *Topics in Fluorescence Spectroscopy: Vol. 2. Principles*, (Ed: J. R. Lakowicz), Kluwer Academic/Plenum Publishers, New York **1999** 53; (b) X. Z. Feng, Z. Zhang, L. J. Yang, C. Wang, C. L. Bai, *Talanta* **1998**, 47, 1223.
- [44] (a) J. H. Tang, F. Luan, X. G. Chen, *Bioorg. Med. Chem.* **2006**, 14, 3210; (b) B. Annaraj, M. A. Neelakantan, *Eur. J. Med. Chem.* **2015**, 102, 1.
- [45] P. Krishnamoorthy, P. Sathyadevi, A. H. Cowley, R. R. Butorac, N. Dharmaraj, *Eur. J. Med. Chem.* **2011**, 46, 3376.
- [46] A. Bujacz, *Acta Crystallogr. D* **2012**, 68, 1278.

SUPPORTING INFORMATION

Additional Supporting Information may be found online in the supporting information tab for this article.

How to cite this article: Balakrishnan C, Theetharappan M, Kowsalya P, Natarajan S, Neelakantan MA, Mariappan SS. Biocatalysis, DNA-protein interactions, cytotoxicity and molecular docking of Cu(II), Ni(II), Zn(II) and V(IV) Schiff base complexes. *Appl Organometal Chem.* 2017;e3776. <https://doi.org/10.1002/aoc.3776>